

A facile route for preparation of magnetic biomass activated carbon with high performance for removal of dye pollutants

Hao Luo¹ · Shengxiao Zhang¹ · Xiaoyan Li¹ · Qiang Xu¹ · Junshen Liu¹ · Zhenhua Wang²

Received: 4 November 2016 / Accepted: 4 May 2017 / Published online: 18 May 2017
© Springer-Verlag Berlin Heidelberg 2017

Abstract A novel and simple method for preparing magnetic biomass activated carbon (BAC) was developed. The BAC was prepared by decomposing fallen leaves, and magnetic nanoparticles were grown in situ on BAC using solvothermal method. The prepared magnetic BAC was characterized with FT-IR, XRD, vibrating sample magnetometer, thermogravimetric apparatus, SEM, and high-resolution transmission electron microscope, and results indicate that BAC and magnetic nanoparticles were combined together successfully. To investigate the adsorption ability of the composites, several dyes were selected as sample pollutants, and the sorbent showed high adsorption capacity for the dyes. The solution pH had no significant effect on the adsorption in the range of 5–9. The adsorption behavior of magnetic BAC for dyes followed the Langmuir isotherm model, and the adsorption capacity of congo red, neutral red, and methyl green were 396.8, 171.2, and 403.2 mg/g, respectively. The maximum adsorption capacity in natural water showed no obvious decrease, indicating the strong anti-interference ability of the sorbents. The Gibbs free energy calculated from the thermodynamics data was negative, demonstrating that the adsorption of these dyes on the magnetic BAC was spontaneous. The

magnetic BAC showed a great potential for the removal of dye pollutants from environment water.

Keywords Biomass activated carbon · Magnetic nanoparticle · Adsorption · Dyes

Introduction

Dye is one category of organic pollutant in the industrial wastewater. The water pollution caused by dye wastewater discharge has caused great attention in recent years. Studies have shown that the dye pollutants can lead to many diseases, such as cancer, anemia, and breathing disorders (Zhang et al. 2014a). It is commonly recognized that dye wastewater was extremely difficult to treat with biodegradation (Gao et al. 2015) due to its high content of organic matter, high concentration, and deep chromaticity. Many methods have been developed for the treatment of dye pollutants, such as adsorption, membrane filtration, photocatalytic degradation, flocculation, and chemical/electro-oxidation (Wang et al. 2015). However, all treatment methods mentioned above have obvious disadvantages, such as high cost and complicated process.

Recently, the application of nanomaterials in environmental remediation becomes a focus due to their excellent properties, such as good absorption property, high surface area, and special photoelectric properties. However, the small size of nanoparticle results in the difficulty of its separation from solution, which limits its application in water treatment. The magnetic nanomaterials provide a solution to this problem since the paramagnetism of magnetic nanomaterials can make them be easily separated from the aqueous solution under external magnetic field. The application of magnetic nanomaterials for removal of various pollutants is widely explored (Casado-Carmona et al. 2016; Zhang et al. 2016;

Responsible editor: Guilherme L. Dotto

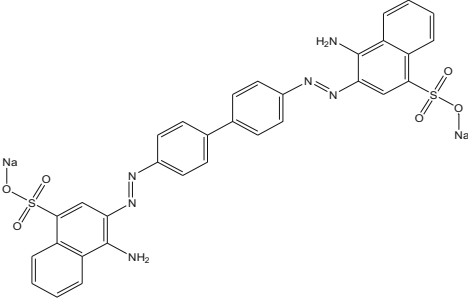
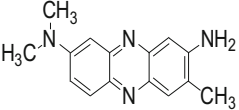
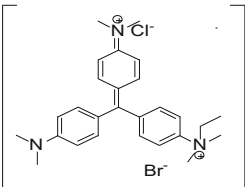
✉ Shengxiao Zhang
beijingzxsx@163.com

✉ Zhenhua Wang
wzh312@sohu.com

¹ School of Chemistry and Materials Science, Ludong University, Yantai 264025, China

² Shandong Analysis and Tester Center, Shandong Academy of Science, Jinan, China

Table 1 Structure formulas and other information of dyes

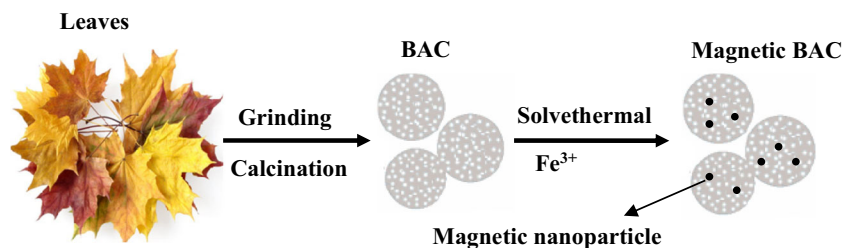
Dyes	Structures formulas	Molecular formulas	Relative molecular mass	Peak wavelength (nm)
Congo red		$C_{32}H_{22}N_6Na_2O_6S_2$	696.68	499.00
Neutral red	 HCl	$C_{15}H_{16}N_4 \cdot HCl$	288.7753	275.50
Methyl green	 ZnCl ₂	$C_{27}H_{35}BrClN_3 \cdot ZnCl_2$	608.78	631.50

Verma et al. 2017; Xiao et al. 2016; Tang et al. 2011; Habuda-Stanić and Nujić 2015; Boopathy et al. 2013). Effective though these methods are, many disadvantages still remain to be overcome, such as complicated preparation processes, high cost and toxic reagents, and low removal efficiency. Therefore, it is necessary to develop a simple and environmentally friendly preparation method for novel magnetic materials to remove pollutants effectively.

Activated carbon (AC) with a good chemical stability, a developed pore structure, and a high specific surface area (Faria et al. 2004; Oh et al. 2015) has been widely used to remove pollutants from wastewater and gas. The adsorption of pollutants in water, such as heavy metals, natural organic matters, pesticides, and organic micro-pollutants, has been reported recently (Li et al. 2015; Humbert et al. 2008; Hadi et al. 2015a; Salman et al. 2011).

Adsorption properties of AC rely on raw materials, manufacturing method, and activating agent (Emami and Azizian 2014). Almost all of the carbon materials can be used to prepare the activated carbons. Generally, the resources of AC can be divided into three categories: (1) biomass materials, such as wood, shells (Boopathy et al. 2013), rice husk (Alvarez et al. 2014), litchi shells (Zhang et al. 2014b), nuts (Şencan et al. 2015), and fruit stones (Bouhamed et al. 2016); (2) mineral materials including coal, activated carbon, oil, and petroleum coke; and (3) some wastes such as cotton woven waste (Zheng et al. 2014), waste tires (Belgacem et al. 2014), waste tea (Inal et al. 2015), and sludge (Hadi et al. 2015b). Main compositions of dry leaves are carbohydrates, proteins, and fibers, all of which can act as important sources of carbon (Biswal et al. 2013). Dry leaves have been applied for the synthesis of AC by high-temperature calcination and chemical

Fig. 1 Schematic diagram for the route of preparing magnetic biomass activated carbon



activation (Biswal et al. 2013; Xu et al. 2014). A few studies also reported that AC produced from leaves can be used as supercapacitor material (Biswal et al. 2013; Peng et al. 2013) and for the removal of dyes such as malachite green (Akar et al. 2013) and methylene blue (Dural et al. 2011). Using biomass materials to prepare AC can not only reduce costs but also eliminate possible pollution to water and air.

Various methods were developed for introducing magnetic material on AC, including wet impregnation (Park et al. 2015), co-precipitation method (Oh et al. 2015), one-step method synthesis (Zhang et al. 2015), and the microwave hydrothermal treatment technique (Yürüm et al. 2014). However, there are some shortcomings for these synthesized magnetic AC reported in the literature, for example, the loaded magnetic nanoparticles were not uniform or easy to detach from the AC surface, and the pores of AC were easily blocked, which limits their application.

In this work, fallen leaves, a recycling waste biomass, were utilized as carbon resource to prepare biomass activated carbon (BAC). Then, magnetic iron oxide nanoparticles were grown in situ on the surface of BAC using solvothermal method. The prepared novel magnetic BAC was applied for the removal of dye pollutants in the water. Three organic dyes were selected as sample pollutants to study the adsorption behavior of the materials, including cationic dyes (methyl green and neutral red) and anionic dye (congo red). These dyes have a large consumption in the textile industry, and the discharged wastewater containing high concentrations of these dyes will pose a large threat on the environment. The

removal methods of these dyes were widely studied (Zhu et al. 2017; Xie and Xiong 2017; Wang et al. 2013; Farghali et al. 2013). Their molecular structures and some other information are shown in Table 1.

Experimental

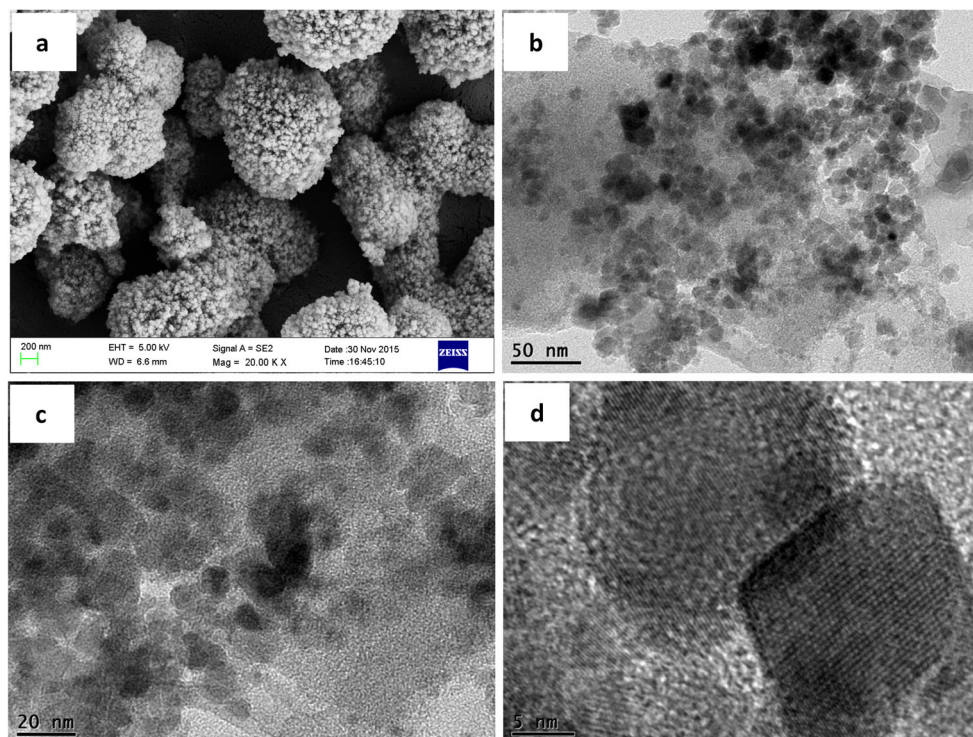
Materials and reagents

All the reagents used in the experiment were of analytical reagents without further purification. Anhydrous FeCl_3 , anhydrous CH_3COONa , and diethylene glycol (DEG) were all bought from Tianjin Bodi Chemical Industry Co., Ltd., and the fallen leaves were from the *Platanus orientalis* in our campus.

Preparation of sorbents

The BAC was prepared with the high-temperature calcination method. *Platanus orientalis* leaves were cleaned up with deionized water and dried in an oven at 50 °C for 12 h. The leaves were grinded by the planet ball grinding mill in order to get leaf powder, and then the powder was sifted with a 60-mesh-size molecular sieve. The leaf powder was heated in an alumina crucible at 800 °C for 5 h under argon atmosphere at a heating rate of 5 °C/min in a tube furnace, and then naturally cooled to room temperature with the color of the leaf powder turning from yellow into black.

Fig. 2 a SEM and b–d TEM images of the $\text{Fe}_3\text{O}_4/\text{BAC}$ (1:2) material



The preparation process of magnetic BAC was as follows: BAC (0.9 g), anhydrous FeCl_3 (0.972 g), and anhydrous CH_3COONa (1.5 g) were added into 60 mL DEG, and the mixture was agitated under heating till it turned into a homogeneous solution. Then, the solution was transferred into a PTFE-lined autoclave, and maintained at 200 °C for 24 h. After the autoclave cooled to room temperature, the mixture was separated with a powerful Rb-Fe-B magnet and rinsed thoroughly with ethanol for three times to remove residual impurities. Finally, it was dried at 35 °C to get magnetic BAC with a Fe_3O_4 /BAC weight ratio of 1:2. If the amount of BAC was adjusted to 1.8 g and other conditions remained the same, the magnetic BAC with a Fe_3O_4 /BAC weight ratio of 1:4 was obtained. The synthetic route diagram is presented in Fig. 1.

Characterization of sorbents

The particle size and the surface morphology analysis were carried out on a SUPPA 55 scanning electron microscopy (SEM) system (Zeiss, Germany) and a high-resolution transmission electron microscope (HR-TEM) of FEI Tecnai G20

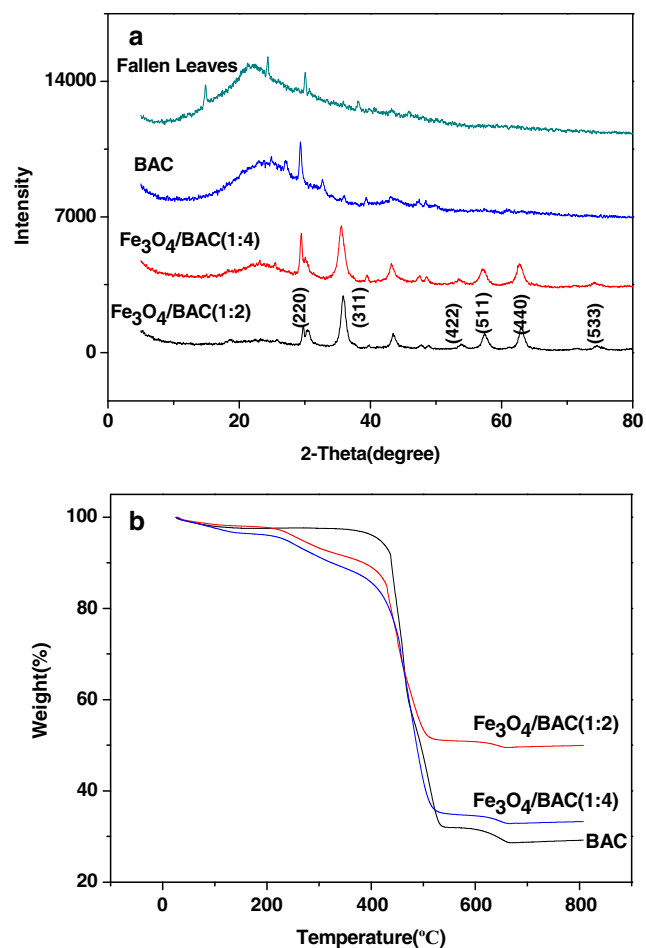


Fig. 3 a XRD and b TGA curves of fallen leaves, BAC, Fe_3O_4 /BAC (1:2) material, and Fe_3O_4 /BAC (1:4) material

(FEI Corp., USA) with an acceleration voltage of 200 kV. The crystalline phase of the final product was identified using an X-ray diffractometer (XRD; Rigaku D/max-2500VPC) with Ni-filtered Cu-K α radiation. Fourier transform infrared (FT-IR) spectra were taken in KBr pressed pellets on a NEXUS 670 FT-IR Spectrometer (Madison, WI, USA). Thermo-gravimetric analysis (TGA) was carried out with a SDT Q600 thermo-gravimetric apparatus (TA Instruments, USA). Magnetic property of the magnetic BAC was analyzed using a vibrating sample magnetometer (VSM, LDJ9600).

Batch adsorption experiments.

The dye adsorption experiments were carried out in 100-mL polypropylene bottles containing 25 mL aqueous solution, and the concentration of the sorbent was kept at 0.5 g/L. To investigate the effect of pH on adsorption, the solution pH was adjusted in the range of 3–9 with HCl and NaOH, and the suspension was shaken at 30 °C for 24 h. Adsorption

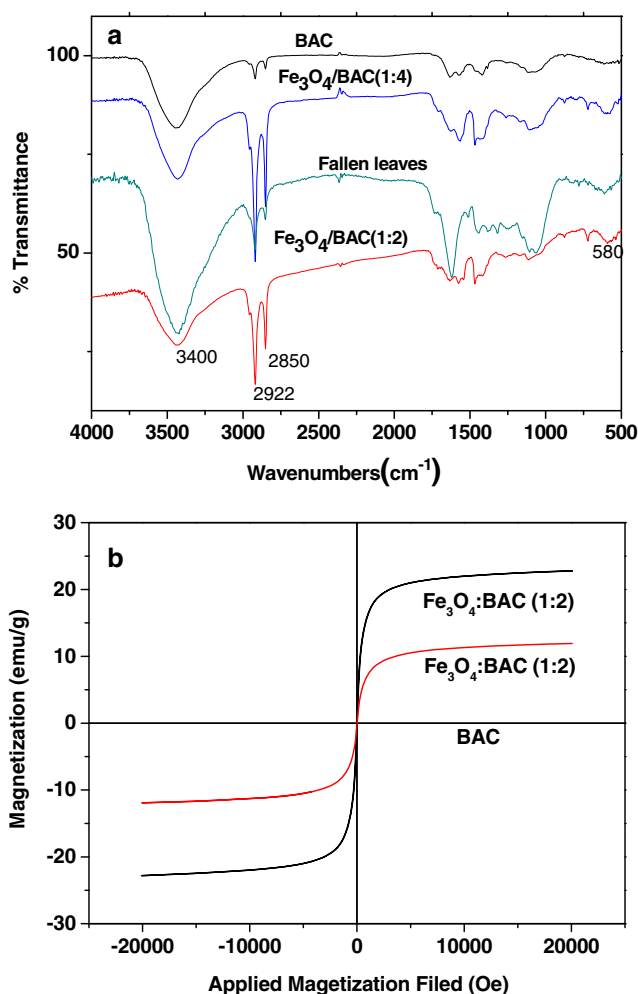


Fig. 4 a FT-IR spectra and b magnetization hysteresis loops of fallen leaves, BAC, Fe_3O_4 /BAC (1:2) material, and Fe_3O_4 /BAC (1:4) material

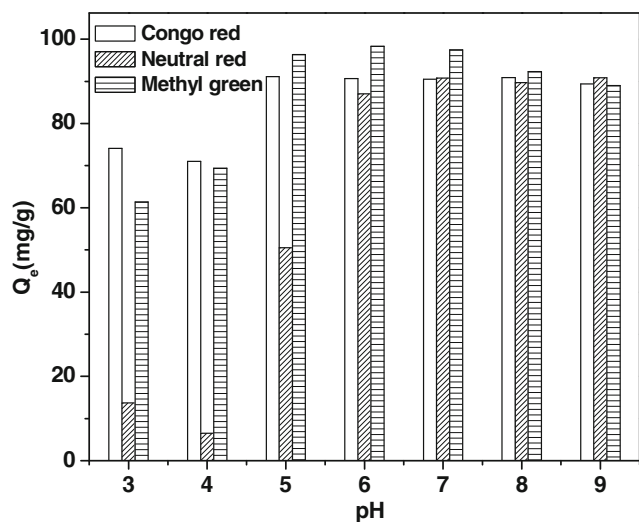


Fig. 5 Effect of pH on removal efficiencies of methyl green, congo red, and neutral red with the Fe₃O₄/BAC (1:2) sorbent

isotherms were obtained by varying the initial concentration of target dye pollutants. The initial concentrations of congo red, neutral red, and methyl green were in the range of 30–250, 30–120, and 20–240 mg/L, respectively. To detect the adsorption rate of dyes, a 200-mL aqueous solution containing 0.1 g sorbent was shaken at 30 °C, and the original concentrations of congo red, neutral red, and methyl green were set at 100, 70, and 70 mg/L, respectively. Ten milliliters of suspension was taken to determine the dye concentration at different time intervals. Various thermodynamic parameters were also determined, and the initial concentrations of dye were all 20 mg/L, and temperatures were set at 20, 30, and 40 °C, respectively. The application of the Fe₃O₄/BAC (1:2) material for removal of dyes from natural water was tested using tap water, lake water, and sea water as matrices.

After adsorption, the bottle was placed on a magnet for 5 min to separate the Fe₃O₄/BAC sorbent from aqueous solution. When the solution became clear, the supernatant was taken for analysis, and the concentrations of dyes were measured by a UV-Vis spectrophotometer (UV-2550, Shimadzu) at their corresponding maximum absorption wavelength (Table 1).

Collection of natural water samples

All natural water samples were obtained from different areas of Yantai, Shandong province. Tap water sample was taken from our lab, and lake water sample was collected from a lake in our campus. Sea water sample was obtained from coastal waters of Yantai. All samples were collected randomly and filtered to remove suspended particles.

Results and discussion

Characterization of Fe₃O₄ and Fe₃O₄/BAC

The surface morphology of the Fe₃O₄/BAC (1:2) material was studied with SEM and TEM. Figure 2 shows SEM (Fig. 2a) and TEM (Fig. 2b–d) images of the composite. As shown in Fig. 2a, fine particles of Fe₃O₄ deposited onto the surface of BAC, and nearly spherical nanoparticles distributed uniformly on large particles of BAC. The surface of the composite was rough and porous. Figure 2b shows clearly that black Fe₃O₄ particles deposited onto the surface of the BAC, and as shown in Fig. 2c, the Fe₃O₄ nanoparticles were nearly spherical with uniform distribution of particle size. Figure 2d shows the high-resolution image of Fe₃O₄ nanoparticles. A clear lattice structure could be observed, and the distance between adjacent atomic lattices was 0.4844 nm, which corresponded to the lattice plane (111) of Fe₃O₄. The results from SEM and TEM showed that BAC and iron oxide were compounded together. Figure 3a shows the XRD analysis of fallen leaves, BAC, Fe₃O₄/BAC (1:2) material, and Fe₃O₄/BAC (1:4) material. The XRD pattern of fallen leaves and BAC showed a typical amorphous structure with the two peaks at about 23.3° and 43.8° (Oh et al. 2015; Biswal et al. 2013). In the Fe₃O₄/BAC compositions, the characteristic peaks of BAC could be observed, and other peaks at 30.10°, 35.45°, 43.08°, 53.45°, 56.98°, 62.57°, and 74.02° could be ascribed to (220), (311), (400), (422), (511), (440), and (533) planes of the Fe₃O₄ particles (JCPDS 65-3107), respectively. Compared with Fe₃O₄/BAC (1:4), the Fe₃O₄/BAC (1:2) diffraction peaks became narrower and sharper with the increase of the Fe₃O₄/BAC mass ratio, which might be because of the increase of particle size and crystallinity.

Thermogravimetric analysis of BAC, Fe₃O₄/BAC (1:2), and Fe₃O₄/BAC (1:4) was carried out, and the results are

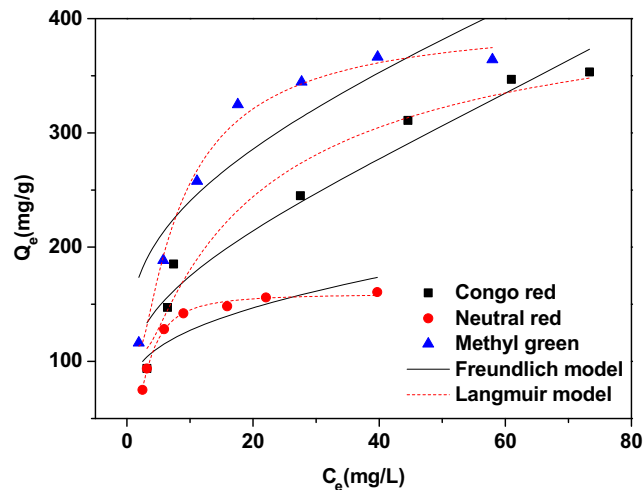


Fig. 6 Adsorption isotherms of methyl green, congo red, and neutral red on the Fe₃O₄/BAC (1:2) sorbent

Table 2 Langmuir and Freundlich isotherm parameters for dye adsorption on Fe₃O₄/BAC (1:2) material

Pollutants	Water matrix	Langmuir model			Freundlich model		
		θ (mg/g)	b (g/mL)	R^2	K_F (mL ^{1/n} μg ^{1-1/n})	n	R^2
Congo red	Pure water	396.8	0.088	0.984	69.85	2.572	0.932
	Tap water	400.5	22.494	0.974	42.37	1.856	0.951
	Lake water	386.5	23.645	0.953	27.58	1.445	0.981
	Sea water	404.8	12.453	0.998	49.44	1.934	0.970
Neutral red	Pure water	171.2	0.414	0.998	18.48	3.879	0.799
	Tap water	160.8	8.112	0.993	34.57	2.612	0.949
	Lake water	146.2	4.534	0.991	44.28	3.117	0.942
	Sea water	166.1	9.321	0.960	31.48	2.367	0.959
Methyl green	Pure water	403.2	0.188	0.997	74.15	1.804	0.975
	Tap water	386.1	6.004	0.996	30.01	1.410	0.974
	Lake water	390.6	14.148	0.982	68.82	2.536	0.982
	Sea water	375.9	8.026	0.979	109.87	3.516	0.948

shown in Fig. 3b. Three steps of weight loss were observed on the TGA curve of BAC. About 3% of weight loss occurred from room temperature to around 140 °C, which was attributed to evaporation of absorbed water. From 370 to 535 °C, about 65% of weight loss was shown in the TGA curve due to the combustion of carbon material. From 600 to 660 °C about 3% of weight loss was related to the further volatilization of the residual substance. The TGA curves of the Fe₃O₄/BAC (1:2) and Fe₃O₄/BAC (1:4) materials also showed three stages of weight loss. The weight of Fe₃O₄/BAC decreased slightly in the temperature ranging from room temperature to around 100 °C. It might be caused by evaporation of the absorbed water. The second weight loss corresponded to the combustion of carbon which occurred from 210 to around 520 °C. The weight losses of Fe₃O₄/BAC (1:2) and Fe₃O₄/BAC (1:4) were about 45 and 57%, respectively, which was expected due to the high content of carbon of the latter. The third weight loss was related to the further volatilization of the residual substance such as Fe₃O₄.

Table 3 Adsorption capacity of dyes on reported sorbents

Adsorbents	Adsorbates	Q_{max} (mg/g)	References
Kaolin clays	Congo red	7.27	(Vimonses et al. 2009)
Bentonite	Congo red	158.70	(Bulut, Özacar and Şengil 2008)
Halloysite nanotubes	Neutral red	65.45	(Luo et al. 2010)
Rice husk	Neutral red	32.37	(Zou et al. 2012)
NiFe ₂ O ₄ -CNTs	Methyl green	113.43	(Bahgat et al. 2012)
Graphene sheets	Methyl green	312.80	(Farghali et al. 2013)

The functional groups on the surface of the fallen leaves, BAC, Fe₃O₄/BAC (1:2) material, and Fe₃O₄/BAC (1:4) material were characterized with FT-IR. As shown in Fig. 4a, the spectra of Fe₃O₄/BAC (1:2) and Fe₃O₄/BAC (1:4) materials both showed strong peaks at 580 cm⁻¹, which was ascribed to the Fe-O bond (Zhang et al. 2014a). These spectra also showed peaks at 2850 and 2922 cm⁻¹, which came from the characteristic -CH₂- or -CH₃, indicating the existence of some groups of AC (Wang et al. 2008). The characteristic band at 3400 cm⁻¹ was present in all the spectra, but compared with BAC, the peak of Fe₃O₄/BAC (1:2) and Fe₃O₄/BAC (1:4) materials became broader, which might be caused by the water absorption. The results from FT-IR showed that BAC and iron oxides were compounded together.

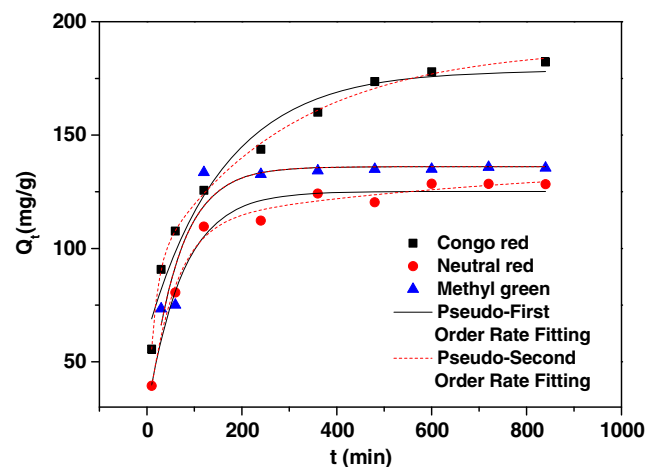
**Fig. 7** Curves of pseudo-first-order kinetic fitting and pseudo-second-order kinetic fitting of dyes on the Fe₃O₄/BAC (1:2) sorbent

Table 4 Pseudo-first-order rate constants and pseudo-second-order rate constants for dye adsorption on Fe₃O₄/BAC (1:2) sorbent

Pollutants	Pseudo-first-order rate constants		Pseudo-second-order rate Constants		
	<i>K</i> ₁ (g/mg min)	<i>R</i> ²	<i>K</i> ₂ (g/mg min)	<i>h</i> (mg/g min)	<i>R</i> ²
Congo red	5.32 × 10 ⁻³	0.957	1.02 × 10 ⁻⁴	3.78	0.997
Neutral red	5.48 × 10 ⁻³	0.971	2.25 × 10 ⁻⁴	4.01	0.998
Methyl green	8.04 × 10 ⁻³	0.866	2.89 × 10 ⁻⁴	5.71	0.997

In order to determine the magnetic property, VSM was used to measure the hysteresis loops of BAC, Fe₃O₄/BAC (1:2), and Fe₃O₄/BAC (1:4), and the results are provided in Fig. 4b. BAC materials exhibited no magnetic behavior. There were no hysteresis in the hysteresis loops of Fe₃O₄/BAC (1:2) and Fe₃O₄/BAC (1:4) materials, and the remanence and coercivity were nearly zero, showing a typical superparamagnetic behavior. The maximal saturation magnetization of Fe₃O₄/BAC (1:2) and Fe₃O₄/BAC (1:4) was 22.7 and 11.9 emu g⁻¹, respectively, and it decreased with the increase of mass ratio of nonmagnetic BAC. Because of the large saturation magnetization and superparamagnetic property of the Fe₃O₄/BAC material, it could be easily separated from solution with a magnet and redispersed rapidly as soon as the magnet was taken away, which facilitated collection and regeneration of the materials. Considering the magnetic separation and adsorption properties together, the Fe₃O₄/BAC (1:2) material was selected as sorbent for the next adsorption experiment.

Effect of solution pH on removal efficiency

The effect of solution pH on dye adsorption was investigated in the range of 3 to 9, and the initial concentrations of congo red, neutral red, and methyl green were all set at 50 mg/L. The results are shown in Fig. 5. As we could see, with the increase of the solution pH, the adsorption capacity of congo red gradually increased at first, then leveled off in the range of 5–9. A

similar phenomenon was observed with neutral red and the methyl green. The results could be explained by electrostatic interactions. For the cationic dye, neutral red, and methyl green, the decrease of adsorption capacity might be attributed to the dye protonation effect in the acidic condition. With the increase of solution pH, the number of ionizable surface sites of the Fe₃O₄/BAC material increased, leading to enhanced adsorption capacity. For the anionic dye, congo red, when pH was less than 5, the relatively low adsorption capacity might be caused by the poor combination between congo red and the sorbent. The larger adsorption capacity obtained at pH = 5 was because the amino contained in congo red could neutralize a small amount of protons. The results showed that the Fe₃O₄/BAC (1:2) sorbent was suitable for dye removal under a wide range of solution pH.

Adsorption isotherms

The adsorption isotherms of the Fe₃O₄/BAC (1:2) material for congo red, neutral red, and methyl green were measured at 303 K, and the initial concentrations of them were set from 30 to 180, 30 to 120, and 20 to 240 mg/L, respectively. The equilibrium adsorption data are shown in Fig. 6. With the increase in pollutant concentrations, the adsorption capacity increased sharply in the first stage, and then attained a balance. It can be observed that Fe₃O₄/BAC (1:2) showed high adsorption capacity for all three dyes, which resulted from the strong adsorption property of BAC. The adsorption data of dyes on the Fe₃O₄/BAC (1:2) material were analyzed with Langmuir and Freundlich isotherm models:

$$q_e = \frac{\theta b C_e}{1 + b C_e} \tag{1}$$

$$q_e = K_F C_e^{1/n} \tag{2}$$

where *q_e* (mg/g) and *C_e* (mg/L) are the equilibrium adsorption capacity and the equilibrium concentration, respectively; *θ* (mg/g) is the maximum adsorption capacity and *b* (L/mg) is

Table 5 Thermodynamic parameters for adsorption of dyes onto Fe₃O₄/BAC (1:2) sorbent

Dyes	<i>C</i> ₀ (mg/L)	<i>C_e</i> (mg/L)			ΔH^θ (kJ/mol)	ΔS^θ (J/mol K)	ΔG^θ (kJ/mol)		
		At 293 K	At 303 K	At 313 K			At 293 K	At 303 K	At 313 K
Congo red	20	0.156	0.231	0.369	-33.18	-53.69	-17.44	-16.91	-16.37
Neutral red	20	4.895	2.096	0.982	70.08	254.5	-4.49	-7.03	-9.58
Methyl green	20	1.651	0.941	0.225	78.44	305.63	-11.11	-7.58	-17.22

the equilibrium adsorption constant. K_F ($\text{mL}^{1/n} \mu\text{g}^{1-1/n}$) and n are the Freundlich constants.

The fitted parameters of these two models are listed in the Table 2. The correlation coefficients (R^2) of the Langmuir model for all dyes were over 0.99, and those of Freundlich models were in the range of 0.799–0.975. Figure 6 shows the linear fitting of the Langmuir isotherm model, and it exhibited good linearity. The adsorption data corresponded well with the Langmuir model, indicating that the adsorption of dyes on the $\text{Fe}_3\text{O}_4/\text{BAC}$ sorbent happened on a single monolayer. Calculated from the Langmuir adsorption isotherm, the maximum adsorption capacity of congo red, neutral red, and methyl green were 396.8, 171.2, and 403.2 mg/g, respectively. Thus, it suggested that the present $\text{Fe}_3\text{O}_4/\text{BAC}$ (1:2) material could be an excellent sorbent for dye pollutants compared with other sorbents shown in Table 3.

Adsorption kinetics

The adsorption kinetics of dyes on the $\text{Fe}_3\text{O}_4/\text{BAC}$ (1:2) material was performed by contacting with 70 mg/L of methyl green, 100 mg/L of congo red, and 70 mg/L of neutral red solution. Figure 7 shows the uptake rate of dyes at the temperature of 303 K. As can be seen, the adsorption capacity was enhanced quickly initially, then slowed down, and finally reached equilibrium when the adsorption capacity was no longer changing. In order to investigate the rate mechanism of the adsorption of dyes on the $\text{Fe}_3\text{O}_4/\text{BAC}$ (1:2) material, the pseudo-first-order kinetic model and the pseudo-second-order kinetic model were applied to describe the kinetic data, and its linear model is shown below:

$$\log(q_e - q_t) = \log q_e - \frac{k_1 t}{2.303} \quad (3)$$

$$\frac{t}{q_t} = \frac{1}{k_2 q_e^2} + \frac{1}{q_e} t \quad (4)$$

where k_1 and k_2 (g/mg min) are the rate constants of adsorption, q_t (mg/g) is the adsorption amount of dye at any time, and q_e (mg/g) is the equilibrium adsorption capacity, and the initial adsorption rate h (mg/g min) can be defined as

$$h = k q_e^2 (t \rightarrow 0) \quad (5)$$

Both k and h can be determined from the slope and intercept of the t/q_t -versus- t plot, and the results are presented in Table 4. As shown in Fig. 7, the fitted curves of the pseudo-second-order kinetic model showed better linear relationship than the pseudo-first-order kinetic model, with a linear

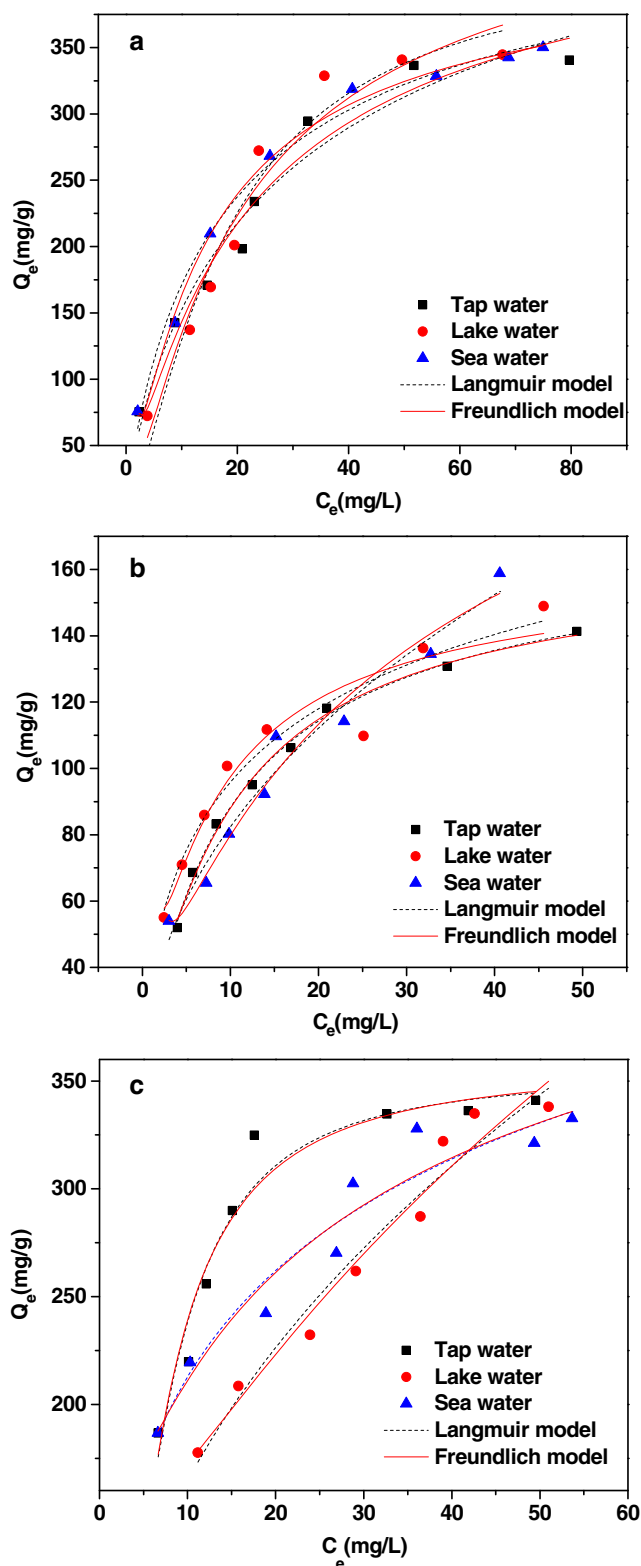


Fig. 8 Adsorption isotherms of **a** congo red, **b** neutral red, **c** methyl green, on the $\text{Fe}_3\text{O}_4/\text{BAC}$ (1:2) sorbent from the natural water samples

correlation coefficient (R^2) over 0.997. The $\text{Fe}_3\text{O}_4/\text{BAC}$ (1:2) sorbent exhibited fast adsorption rate and high adsorption efficiency for dye pollutants.

Adsorption thermodynamics

Furthermore, the influence of temperature on dye adsorption was also discussed. The thermodynamic parameters can be obtained from the slope of the linear plot of $\ln K_c$ versus $1/T$, and their equations are shown below:

$$K_C = \frac{Q_e}{C_e} \tag{6}$$

$$\ln K_C = \frac{\Delta S^\theta}{R} - \frac{\Delta H^\theta}{RT} \tag{7}$$

$$\Delta G^\theta = \Delta H^\theta - T\Delta S^\theta \tag{8}$$

where Q_e (mg/g) and C_e (mg/L) are the equilibrium adsorption capacity and the equilibrium concentration, respectively; K_c and T are the distribution coefficient and solution temperature, and R is the gas constant (8.314 J/mol K). ΔG^θ (kJ/mol), ΔH^θ (kJ/mol), and ΔS^θ (J/mol K) are the changes in Gibbs free energy, enthalpy, and entropy under standard states, respectively. The value of ΔH^θ and ΔS^θ could be obtained from the slope of the linear plot of $\ln K_c$ versus $1/T$. ΔG^θ could be obtained from Eq. (7). The adsorption data and thermodynamic parameters are listed in Table 5. The following conclusions could be obtained: (1) The values of ΔH^θ and ΔS^θ were -33.18 and -53.69 J/mol K, respectively, and a low temperature was beneficial to the adsorption, indicating that the adsorption of congo red onto the $\text{Fe}_3\text{O}_4/\text{BAC}$ (1:2) sorbent was an exothermic process. The negative values of ΔG^θ confirmed that the adsorption is a spontaneous process. (2) With the increase of temperature, the adsorption capability of neutral red on $\text{Fe}_3\text{O}_4/\text{BAC}$ (1:2) increased slightly, indicating it is an endothermic process. This was also confirmed by the positive ΔH^θ values. The positive ΔS^θ values confirmed that the adsorption is a chaotic degree increasing process. The negative values of ΔG^θ further suggested that the adsorption is a spontaneous process. Similar results were also found for methyl green.

Environmental implication

The application of the $\text{Fe}_3\text{O}_4/\text{BAC}$ (1:2) material for the removal of dyes from natural water was tested with tap water, lake water, and sea water. The equilibrium adsorption data and the parameters associated with Langmuir and Freundlich models are given in Fig. 8 and Table 2, respectively. The adsorption data were also corresponded well with the Langmuir model, and the maximum adsorption capacity in natural water showed no obvious decrease compared with pure water, indicating the strong anti-interference ability of the sorbent. The $\text{Fe}_3\text{O}_4/\text{BAC}$ material displayed great potential in dye removal from the actual water sample.

Conclusions

The magnetic BAC reported in this work could be prepared by magnetic nanoparticles grown in situ on the surface of BAC from fallen leaves, and it was applied for dye pollutant removal. The raw material and chemicals were easily obtained and were low cost and environmentally friendly. The magnetic BAC showed strong adsorption ability and large adsorption capacity for dye pollutants in pure water as well as natural water. The research not only showed the potential of using waste biomass resources to mitigate environmental pollution but also opened up a new avenue for using magnetic nanoparticles supported on various substrates to prepare magnetic composites.

Acknowledgements This work was jointly supported by the National Natural Science Foundation of China (21207059, 21171085, 21104030, 21206066, 21277084) and the Natural Science Foundation of Shandong Province (ZR2011BQ012, ZR2016BM27).

References

Akar E, Altinişik A, Seki Y (2013) Using of activated carbon produced from spent tea leaves for the removal of malachite green from aqueous solution. *Ecol Eng* 52:19–27

Alvarez J, Lopez G, Amutio M, Bilbao J, Olazar M (2014) Upgrading the rice husk char obtained by flash pyrolysis for the production of amorphous silica and high quality activated carbon. *Bioresour Technol* 170:132–137

Bahgat M, Farghali AA, Roubay WE, Khedr M, Mohassab-Ahmed MY (2012) Adsorption of methyl green dye onto multi-walled carbon nanotubes decorated with Ni nanoferrite. *Appl Nano* 3(3):1–11

Belgacem A, Rebiai R, Hadoun H, Khemaissia S, Belmedani M (2014) The removal of uranium (VI) from aqueous solutions onto activated carbon developed from grinded used tire. *Environ Sci Pollut R* 21: 684–694

Biswal M, Banerjee A, Deo M, Ogale S (2013) From dead leaves to high energy density supercapacitors. *Energy Environ Sci* 6:1249

Boopathy R, Karthikeyan S, Mandal AB, Sekaran G (2013) Adsorption of ammonium ion by coconut shell-activated carbon from aqueous solution: kinetic, isotherm, and thermodynamic studies. *Environ Sci Pollut R* 20:533–542

Bouhamed F, Elouear Z, Bouzid J, Ouddane B (2016) Multi-component adsorption of copper, nickel and zinc from aqueous solutions onto activated carbon prepared from date stones. *Environ Sci Pollut R* 23: 15801–15806

Bulut E, Özacar M, Şengil IA (2008) Equilibrium and kinetic data and process design for adsorption of Congo Red onto bentonite. *J Hazard Mater* 154(1–3):613–622

Casado-Carmona FA, Alcudia-León M d C, Lucena R, Cárdenas S, Valcárcel M (2016) Magnetic nanoparticles coated with ionic liquid for the extraction of endocrine disrupting compounds from waters. *Microchem J* 128:347–353

Dural MU, Cavas L, Papageorgiou SK, Katsaros FK (2011) Methylene blue adsorption on activated carbon prepared from *Posidonia oceanica* (L.) dead leaves: kinetics and equilibrium studies. *Chem Eng J* 168:77–85

Emami Z, Azizian S (2014) Preparation of activated carbon from date sphate using microwave irradiation and investigation of its

- capability for removal of dye pollutant from aqueous media. *J Anal Appl Pyrol* 108:176–184
- Farghali AA, Bahgat M, Roubay WMAE, Khedr MH (2013) Preparation, decoration and characterization of graphene sheets for methyl green adsorption. *Journal of Alloys & Compounds* 555:193–200
- Faria PC, Orfao JJ, Pereira MF (2004) Adsorption of anionic and cationic dyes on activated carbons with different surface chemistries. *Water Res* 38:2043–2052
- Gao Y, Yue Q, Xu S, Gao B, Li Q, Yu H (2015) Preparation and evaluation of adsorptive properties of micro-mesoporous activated carbon via sodium aluminate activation. *Chem Eng J* 274:76–83
- Habuda-Stanić M, Nujčić M (2015) Arsenic removal by nanoparticles: a review. *Environ Sci Pollut R* 22:8094–8123
- Hadi P, TO MH, Hui CW, Lin CS, McKay G (2015a) Aqueous mercury adsorption by activated carbons. *Water Res* 73:37–55
- Hadi P, Xu M, Ning C, Sze Ki Lin C, McKay G (2015b) A critical review on preparation, characterization and utilization of sludge-derived activated carbons for wastewater treatment. *Chem Eng J* 260:895–906
- Humbert H, Gallard H, Suty H, Croue JP (2008) Natural organic matter (NOM) and pesticides removal using a combination of ion exchange resin and powdered activated carbon (PAC). *Water Res* 42:1635–1643
- Inal IIG, Holmes SM, Banford A, Aktas Z (2015) The performance of supercapacitor electrodes developed from chemically activated carbon produced from waste tea. *Appl Surf Sci* 357:696–703
- Li M, Wang C, O'Connell MJ, Chan CK (2015) Carbon nanosphere adsorbents for removal of arsenate and selenate from water. *Environ Sci: Nano* 2:245–250
- Luo P, Zhao Y, Zhang B, Liu J, Yang Y, Liu J (2010) Study on the adsorption of Neutral Red from aqueous solution onto halloysite nanotubes. *Water Res* 44(5):1489–1497
- Oh WD, Lua SK, Dong Z, Lim TT (2015) Performance of magnetic activated carbon composite as peroxymonosulfate activator and regenerable adsorbent via sulfate radical-mediated oxidation processes. *J Hazard Mater* 284:1–9
- Park HS, Koduru JR, Choo KH, Lee B (2015) Activated carbons impregnated with iron oxide nanoparticles for enhanced removal of bisphenol A and natural organic matter. *J Hazard Mater* 286:315–324
- Peng C, Yan X-B, Wang R-T, Lang J-W, Ou Y-J, Xue Q-J (2013) Promising activated carbons derived from waste tea-leaves and their application in high performance supercapacitors electrodes. *Electrochim Acta* 87:401–408
- Salman JM, Njoku VO, Hameed BH (2011) Adsorption of pesticides from aqueous solution onto banana stalk activated carbon. *Chem Eng J* 174:41–48
- Şencan A, Karaboyacı M, Kılıç M (2015) Determination of lead(II) sorption capacity of hazelnut shell and activated carbon obtained from hazelnut shell activated with ZnCl₂. *Environ Sci Pollut R* 22:3238–3248
- Tang T, Fan H, Ai S, Han R, Qiu Y (2011) Hemoglobin (Hb) immobilized on amino-modified magnetic nanoparticles for the catalytic removal of bisphenol A. *Chemosphere* 83:255–264
- Verma R, Asthana A, Singh AK, Prasad S, Susan MABH (2017) Novel glycine-functionalized magnetic nanoparticles entrapped calcium alginate beads for effective removal of lead. *Microchem J* 130:168–178
- Vimonses V, Lei S, Jin B, Chow CWK, Saint C (2009) Adsorption of congo red by three Australian kaolins. *Appl Clay Sci* 43:465–472
- Wang D-W, Li F, Lu GQ, Cheng H-M (2008) Synthesis and dye separation performance of ferromagnetic hierarchical porous carbon. *Carbon* 46:1593–1599
- Wang W, Li C, Yao J, Zhang B, Zhang Y, Liu J (2013) Rapid adsorption of neutral red from aqueous solutions by Zn₃[Co(CN)₆]₂·nH₂O nanospheres. *J Mol Liq* 184:10–16
- Wang Z, Guo J, Ma J, Shao L (2015) Highly regenerable alkali-resistant magnetic nanoparticles inspired by mussels for rapid selective dye removal offer high-efficiency environmental remediation. *J Mater Chem A* 3:19960–19968
- Xiao Z, Yuan M, Yang B, Liu Z, Huang J, Sun D (2016) Plant-mediated synthesis of highly active iron nanoparticles for Cr (VI) removal: investigation of the leading biomolecules. *Chemosphere* 150:357–364
- Xie H, Xiong X (2017) A porous molybdenum disulfide and reduced graphene oxide nanocomposite (MoS₂-rGO) with high adsorption capacity for fast and preferential adsorption towards Congo red. *Journal of Environmental Chemical Engineering* 5:1150–1158
- Xu J, Chen L, Qu H, Jiao Y, Xie J, Xing G (2014) Preparation and characterization of activated carbon from reedy grass leaves by chemical activation with H₃PO₄. *Appl Surf Sci* 320:674–680
- Yürüm A, Kocabaş-Ataklı ZÖ, Sezen M, Semiat R, Yürüm Y (2014) Fast deposition of porous iron oxide on activated carbon by microwave heating and arsenic (V) removal from water. *Chem Eng J* 242:321–332
- Zhang S, Luo H, Zhang Y, Li X, Liu J, Xu Q, Wang Z (2016) In situ rapid magnetic solid-phase extraction coupled with HPLC-ICP-MS for mercury speciation in environmental water. *Microchem J* 126:25–31
- Zhang S, Tao L, Jiang M, Gou G, Zhou Z (2015) Single-step synthesis of magnetic activated carbon from peanut shell. *Mater Lett* 157:281–284
- Zhang S, Zhang Y, Bi G, Liu J, Wang Z, Xu Q, Xu H, Li X (2014a) Mussel-inspired polydopamine biopolymer decorated with magnetic nanoparticles for multiple pollutants removal. *J Hazard Mater* 270:27–34
- Zhang S, Zheng M, Lin Z, Li N, Liu Y, Zhao B, Pang H, Cao J, He P, Shi Y (2014b) Activated carbon with ultrahigh specific surface area synthesized from natural plant material for lithium–sulfur batteries. *J Mater Chem A* 2:15889–15896
- Zheng J, Zhao Q, Ye Z (2014) Preparation and characterization of activated carbon fiber (ACF) from cotton woven waste. *Appl Surf Sci* 299:86–91
- Zou W, Han P, Li Y, Liu X, He X, Han R (2012) Equilibrium, kinetic and mechanism study for the adsorption of neutral red onto rice husk. *Desalin Water Trea* 12(1-3):210–218
- Zhu H, Jiang R, Li J, Fu Y, Jiang S, Yao J (2017) Magnetically recyclable Fe₃O₄/Bi₂S₃ microspheres for effective removal of Congo red dye by simultaneous adsorption and photocatalytic regeneration. *Sep Purif Technol* 179:184–193